Accepted Manuscript

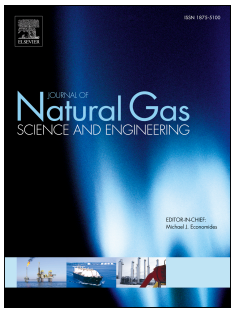

Numerical modelling of acoustic stimulation induced mechanical vibration enhancing coal permeability

Yupeng Jiang, Huilin Xing

PII: S1875-5100(16)30808-3

DOI: 10.1016/j.jngse.2016.11.008

Reference: JNGSE 1918

To appear in: *Journal of Natural Gas Science and Engineering*

Received Date: 24 February 2016

Revised Date: 29 October 2016

Accepted Date: 3 November 2016

Please cite this article as: Jiang, Y., Xing, H., Numerical modelling of acoustic stimulation induced mechanical vibration enhancing coal permeability, *Journal of Natural Gas Science & Engineering* (2016), doi: 10.1016/j.jngse.2016.11.008.

Numerical modelling of acoustic stimulation induced mechanical vibration enhancing coal permeability

Yupeng Jiang, Huilin Xing*

Centre for Geoscience Computing, School of Earth Sciences, The University of Queensland, St Lucia QLD 4072, Australia

*corresponding author: Phone: +61 7 33464093; E-mail: h.xing@uq.edu.au

Abstract: Mechanical vibration is a major effect generated by acoustic stimulation inside a coal sample for enhancing its permeability. The numerical simulation based on the staggered-grid finite differential method (FDM) is applied to simulate 3D wave propagation in a fractured coal. Two parameters, shear wave energy (*SE*) and variable width of cleat (*DW*), are introduced and implemented in the numerical model to explicitly visualise and evaluate the acoustic stimulation effects. The polarized wave induced wave dynamics in a coal sample with a cleat/fracture is numerically simulated and analysed. Especially, the energy trapping and dynamic variation of fracture width in coal for the cleat/fracture with three different filled media (i.e. air, water and weak mineral) are numerically analysed and compared with each other subjected to different incident wave angles, and the optimal stimulation parameters are obtained through such sensitivity analysis. Simulation results show that the coal property (i.e. cleat and its filled media) and incident wave angles are crucial for acoustic stimulation to produce physical damages around coal cleats and enhance the permeability of fractured coal samples.

Keywords: Acoustic stimulation, Mechanical vibration, Energy trapping effect, Permeability, Numerical modelling

1. Introduction

Coal seam gas (CSG), as an unconventional natural gas, is becoming one of the major energy resources around the world. CSG widely exists in pores and fractures/cleats of coal in adsorption state but is difficult to exploit due to the low permeability of coal reservoirs. Therefore, enhancing the permeability and desorption rate of coal are critical for improvement of CSG extraction amount (Gandossi 2013; Li et al., 2015). Many methods such as hydraulic fracturing, high-pressure water jet and blasting vibration (Shen et al., 2012; Li et al., 2009; Shimizu et al., 2011; Li and Xing 2015), have been tested and applied to achieve these goals. The desorption rate and permeability of CSG can also be significantly increased by physical stimulation through changing the thermal field, stress field, electrical and magnetic field (Pan et al., 2012; Azmi et al., 2006; Hol et al., 2011; Charriére et al.,2010; Liu et al., 2006) and their coupling effects. Acoustic wave field stimulation method is relatively new and successfully applied in oil recovery and ultrasonic assisted desorption for removal of aromatic pollutants (Ye et al., 2008; Mohammadian et al., 2013; Alhomadhi et al.,

2014; Naderi et al., 2010). Furthermore, based on these engineering applications, acoustic stimulation method has been put forward to improve CSG extraction rate and permeability. Jiang et al (2015) designed a new apparatus to study the adsorption-desorption characteristics of CSG under ultrasonic stimulation and indicated that the following three factors of the mechanical vibration thermal effect and cavitation generated by acoustic stimulation are responsible for enhancing desorption and permeability. Desorption quantity of CSG is significantly improved through acoustic stimulation (Jiang et al., 2015). Xiao et al (2013) studied CT scans of coal samples after ultrasonic wave processing and identified that both fractures' width and quantity increased, which enhanced the overall permeability of coal samples. The existing research concluded that within the range of ultrasonic attenuation, mechanical vibration is a major factor for permeability enhancement, but its mechanism of whether and how the acoustic stimulation works effectively is still poorly understood and difficult to figure out through the existing laboratory experiments (Xiao et al., 2013; Jiang et al., 2015), and thus numerical simulation based method is chosen as an alternative approach to studying it here.

Numerical simulation of wave dynamics has been widely studied and applied in many cases, which are specified for large scale earthquake numerical modelling (e.g. Chouet, 1986), for dispersion solutions (e.g. Zhu et al., 2004; Valeri Korneev 2008) and for creation of synthetic seismic data (e.g. Wigginst and Helmberge 1973). However, these studies provided limited knowledge for wave-induced mechanical vibration. Because they regarded the wave as a pure signal instead of a form of dynamic force or energy, and lack of proper variables to describe it. The wave dynamic information, especially that at material interfaces (e.g. cleats/fractures) and its linkage to dynamic variation of material permeability are largely ignored, but it is the key for acoustic stimulation that needs be addressed. Hence, our paper focuses on the related investigation and discussion of such dynamic effects during an acoustic stimulation process through the numerical simulation.

This paper is to provide an alternative way to numerically study the mechanical vibration effect especially along the coal cleats/fractures that may disturb the incident ultrasonic waves. It is organized into the following four parts: numerical methodology, computational models, computational results and discussions, conclusions.

2. Numerical methodology

2.1 Governing equations

From the experiments, time-accumulative characteristics of the desorption amount curves and CT scans demonstrated that width (or length) expansion of coal cleats which improved overall permeability of coal samples can only be accomplished after certain stimulation time (Jiang et al., 2015; Xiao et al., 2013). Hence at the initial stimulating stage of the experiment, the ultrasonic wave propagation at the interfaces of a cleat model, or around its surrounding medium, is governed by the elastic wave equation. The following elastic wave equation expressed by particle displacement

vector **u** is applied here:

$$(\lambda+\mu)\nabla(\nabla\cdot\mathbf{u})+\mu\Delta\mathbf{u}=\rho\mathbf{u}_{tt}, \quad (1)$$

where $\mathbf{u_{tt}}$ is the acceleration matrix. Based on the theorem of Helmholtz decomposition, the same wave equation also can be expressed by the scalar potential φ and vector potential $\boldsymbol{\psi}$ of particle displacement (J.d.achenbach 1975; Ashour 2000):

$$\mathbf{u}=\mathbf{u}_p+\mathbf{u}_s, \mathbf{u}_p=\nabla\varphi \text{ and } \mathbf{u}_s=\nabla\times\boldsymbol{\psi}, \quad (2)$$

where $\mathbf{u_p}$ and $\mathbf{u_s}$ are the particle displacement vectors produced by compression wave and shear wave respectively. The λ and μ denote the Lamé parameters where S-wave velocity V_s equals to $(\mu/\rho)^{1/2}$ and P-wave velocity V_p equals to $((\lambda+\mu)/\rho)^{1/2}$.

The first-order velocity-stress staggered-grid finite difference (FVSFD) method has been proved as one of the most effective and efficient algorithms for wave dynamic forward modelling (Madariaga, Virieux and Levander, Robertsson) (Virieux, 1986; Levander, 1988; Robertsson et al., 1994; Robertsson, 1996; Madariaga, 1996). This method is employed in this research to simulate the interface wave field of a cleat model that generated by incident sub-waves to give exact details of the generation of mechanical vibration. The elastic formulation of FVSFD can be written in as

$$\frac{\partial\sigma_{ij}}{\partial t}=\lambda v_{k,k}+2\mu v_{i,i} \text{ if } i=j,$$
$$\frac{\partial\sigma_{ij}}{\partial t}=\mu\cdot\left(v_{i,j}+v_{j,i}\right) \text{ if } i\neq j. \quad (3)$$

And the momentum conservation equation is

$$\rho\frac{\partial v_i}{\partial t}=\sigma_{ij,j}+\rho f_i,(i,j,k=1,2,3), \quad (4)$$

where v_i denotes the component of particle velocity; σ_{ij} denotes the component of stress vector; f_i indicates the terms of external body forces.

2.2 Numerical discretization and stability

Taylor expansion has been employed to solve equation (3) and (4) in 8th order in spatial dimension and 2nd order centred difference in temporal dimension:

$$\frac{\partial f}{\partial x_i}=\frac{1}{\Delta x_i}\sum_{n=1}^{N}C_N^{(N)}\{f[x_i+\frac{\Delta x_i}{2}(2n-1)]-f[x_i-\frac{\Delta x_i}{2}(2n-1)]\}+o(\Delta x_i^{2N}), \quad (5)$$

$$\frac{\partial}{\partial t}f(t)=\frac{f(t+\Delta t/2)-f(t-\Delta t/2)}{\Delta t}, \quad (6)$$

where $i=1,2,3$ and C_N is the coefficients with $2N=8$.The Courant-Friedrichs-Lewy criterion is applied for temporal discretization to avoid numerical instability of the high order finite difference:

$$dt<\frac{dh}{R\sqrt{3}V_{p,max}}, \quad (7)$$

where $V_{p,max}$ denotes the maximum P-wave velocity of the model and R depends on

the order of finite difference operators. The spatial grid distance *dh* is also considered in the criterion, which similarly needs to satisfy the following condition to avoid grid dispersion:

$$dh < \frac{V_{s,min}}{Rf_{max}}, \tag{8}$$

where f_{max} indicate the maximum frequency of incident wave and $V_{s,min}$ represents the minimum S-wave velocity of the model.

2.3 Absorbing boundary conditions

The convolutional perfectly matched layer (CPML) absorbing boundary condition has been introduced to absorb the reflected wave at the boundary of calculation area (Komatitsch and Martin 2007; Zeng et al., 2001). Wave equations are decaying exponentially while propagating through the CPML area. It overcomes the drawback of Dirichlet boundary condition as bellow so that the interface wave field can be isolated and accurately measured from the overall wave field,

$$\mathbf{v}(0) = \mathbf{v}(Nh) = 0, \quad \boldsymbol{\sigma}(0) = \boldsymbol{\sigma}(Nh) = 0. \tag{9}$$

2.4 Numerical validation

The code that developed for this research is firstly tested and benchmarked with wave pressure field analytical solutions under three different input wave functions (Frehner et al., 2010; Fuchs and Müller 1971) as showing in Figure 1.

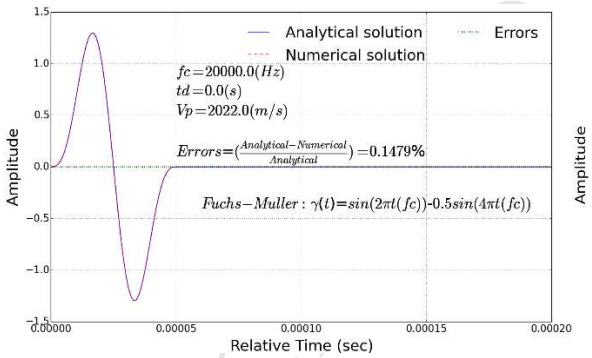

(a)

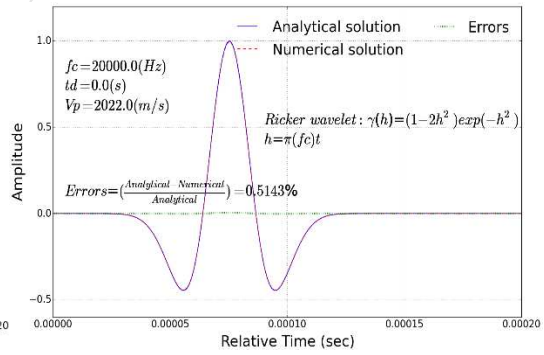

(b)

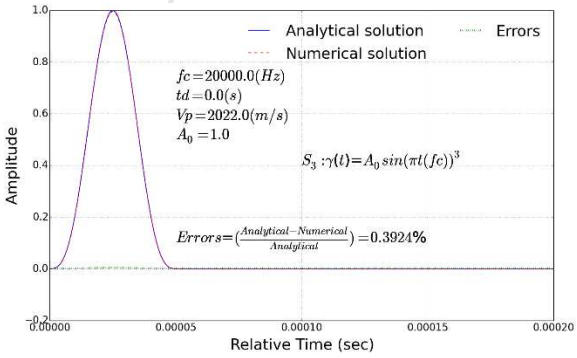

(c)

Figure 1. Comparison of numerical data and analytical data with different source functions. (a) Ricker wavelet, (b) Fuchs-Müller wavelet, (c) S_3 wavelet function.

The pressures are calculated with a central point source in a homogeneous elastic space by using the above numerical and analytical methods and compared with each other (Figure 1), which shows that the numerical solution agrees very well with the analytical ones for all the test cases. This demonstrates the accuracy of the developed code in wave dynamics and will be used here to numerically investigate the acoustic stimulation of coal samples.

3. Computational models

3.1 Cleat model parameters

3.1.1 Geometrical parameters

Due to the irregular geometrical shapes of cleats, it needs to be divided into a small single rectangular hexahedron model with constant geometrical parameters, and by using one single model as the numerical simulation model the interferences of geometrical irregularity has been properly ruled out, so the mechanical vibration effect at interface of coal cleats can be representatively discussed. Figure 2 shows the computational coal model with single cleat inside it, which is set to the same scales of the real coal cleats.

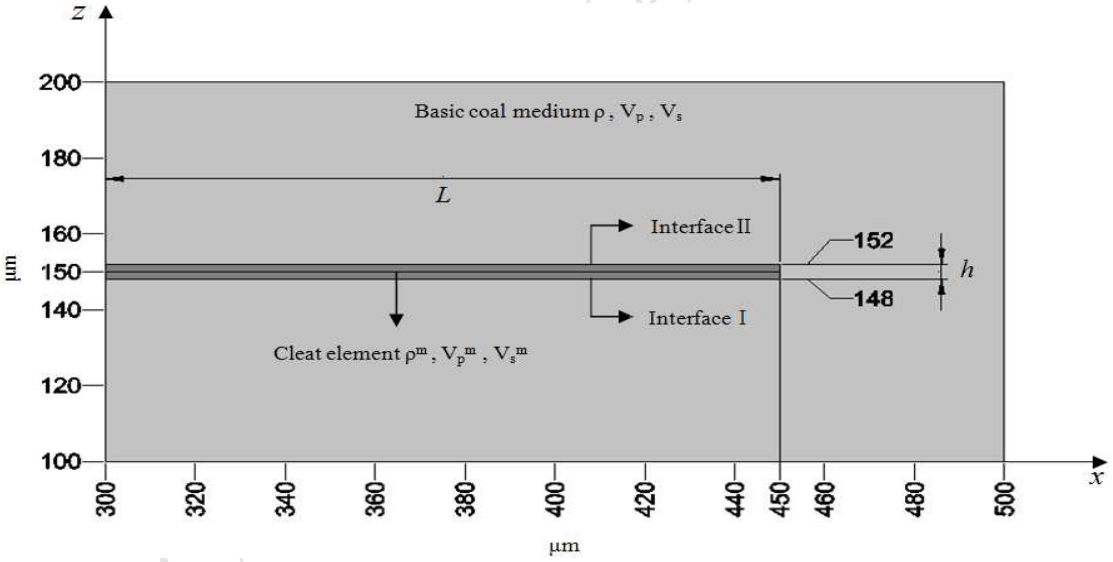

Figure 2. Sketch of the model of cleat model in x-z Cartesian coordinates. Black area represents the cleat model that filled with different medium (water, gas, and calcite). The width of cleat model h=4.0μm and the length L=150.0μm. The gray area represents the basic coal medium that filled with common coal properties. The geometrical parameters of this sketch are actual scales for all simulations. The simulation time interval is 1×10^{-8} s with total time steps of 6000.

3.1.2 Filled media in cleats

In coal reservoirs, coal cleats are filled with various media like single-phase fluids, such as water and mixture of gasses, and solid media such as calcite, mica and

limestone. The differences of material properties (density, velocity, and modulus) between coal cleats and their surrounding coal matrix are actually the key factors for the generation of mechanical vibration. Polarized waves will be produced and propagate along the interface of two different materials if their physical properties fulfil certain criterions. Basically, all of these polarized waves are generated to compensate the discontinuity of physical properties and their wave patterns could be highly affected by the different presence of filled mediums. Therefore, it is imperative to use the representative filled medium for coal cleat model's simulations to get comprehensive details about mechanical vibration. Table.1 shows three groups of properties of model/surrounding medium combination.

Type of filled medium	Basic Solid	Water	Gas	Calcite
P-wave phase velocity V_p (m/s)	2022.00	1403.00	0.001	4120.00
Ratio V^m_p/V_p	/	6.94×10^{-1}	4.95×10^{-7}	2.04
S-wave phase velocity V_s (m/s)	1207.00	0.001	0.001	2030.00
Ratio V^m_s/V_s	/	8.29×10^{-7}	8.29×10^{-7}	1.68
Density ρ (Kg/m^3)	1410.00	1002.00	1.10	2511.00
Ratio ρ^m/ρ	/	7.11×10^{-1}	7.80×10^{-4}	1.78

Table.1 Properties of surrounding medium and filled medium for cleat model.

3.2 Incident wave parameters and analysis

3.2.1 Incident wave length

The frequency and shape of incident waves that generated by the ultrasonic source cannot maintain as constant parameters inside a coal sample. Due to the high heterogeneity of coal, propagation of ultrasonic waves is strongly affected by frequency dispersion and scattering effects in a very short time period and propagating range. This may separate the ultrasonic wave energy into a group of sub-waves with higher frequencies and lower energy. Jiang and Xiao's experimental apparatuses did not measure the changes of ultrasonic wave shape, but the very similar phenomenon was measured and proved by Khosrow Naderi (Naderi et al., 2010). Figure 3 shows a sketch map of experiment data about strong changes of ultrasonic waveform while penetrating through slurry (sand plus water). The frequencies of sub-waves were increased 10^3 times (or even more) than the original frequency. Simple harmonic wave equation (10) is used for illustration. Considering the average energy flux density equation (Vlastislav et al., 2006) and energy conservative law, and ignore any energy attenuation the relation between original acoustic wave and sub-waves can be approximately written as

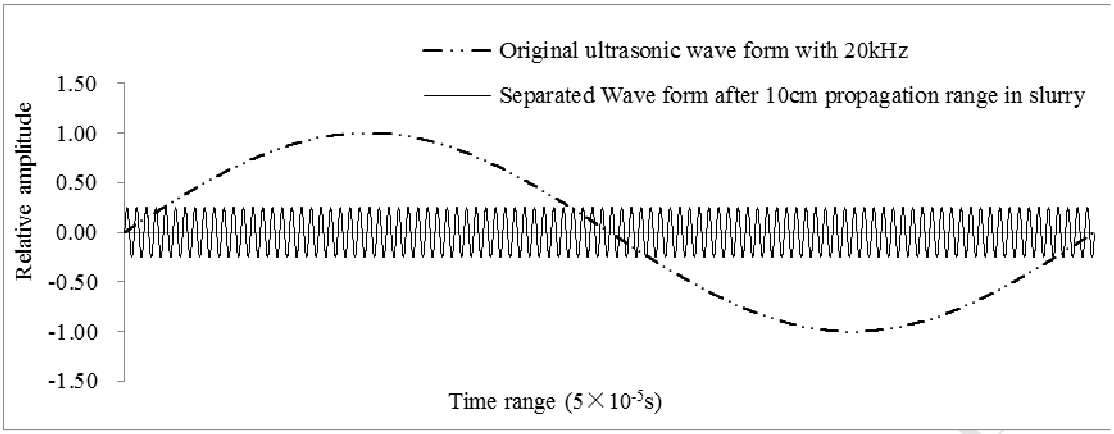

Figure 3. Changes of ultrasonic wave shape and frequency after propagated 10cm in the slurry (sand + water), (Naderi et al., 2010).

$$u = A\sin\omega(t-\frac{x}{C}), \tag{10}$$

$$\frac{1}{2}\rho C\omega^2 A^2 = \sum_{i=0}^{n} a_i^2 \omega_i \rho c_i \frac{1}{T_i}\int_{-x/c_i}^{T_i - x/c_i} \cos^2\omega_i(t-\frac{x}{c_i})dt\,. \tag{11}$$

Since the coal is also showing the similar high heterogeneity like slurry, it is totally reasonable to make the statement that mechanical vibration effect at the interface of coal cleats is generated by sub-waves that divided from the original ultrasonic wave. The wave length of each sub-wave can be calculated from

$$c_i = \frac{\lambda_i}{f_i}. \tag{12}$$

3.2.2 Incident wave angle

During the acoustic stimulation, the coal cleats are constantly getting wave load from various incident wave angles, which deeply affected patterns and levels of mechanical vibration at the interface of cleats. In the research, authors simulated and discussed the differences of mechanical vibration between different incident angles. Figure 4 shows the angle parameters, the black dots represent the source point. Figure 5 shows the 3D image of 0° incident wave and cleat model.

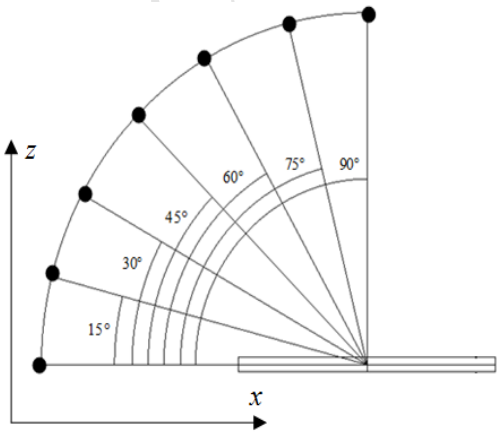

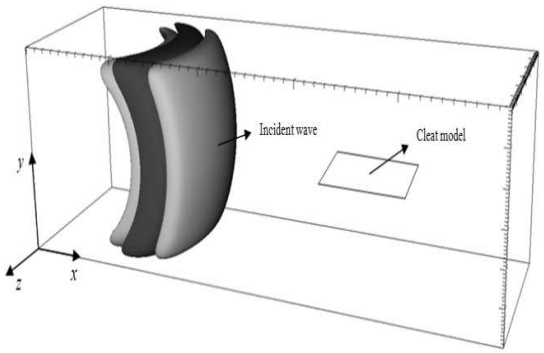

Figure 4. Sketch of the relative positions between 3D cleat element model and incident wave angle α （=0°，15°，30°，45°，60°，75°，90°）. Its visualized ratio is not the actual scale for the element model. The source pressure function that used for all of the simulations are $F(t)=A_0 sin^3(\pi t \times f_c)$,$A_0$=1Mpa. The distant between the source point and center of the model is 2.75×10^2μm. The central frequency of each sub-wave is 20 kHz × 10^3 = 20MHz

Figure 5. Sketch for the cleat model's relative position between the 0° incident wave angle and cleat element in 3D wave propagation snapshot

3.3 Evaluation methods for mechanical vibration

Most research about polarized waves focuses on kinematical features (Zhu and Popovics, 2004; Korneev, 2008; Scholte, 1947), such as velocity, dispersion equation and the variety of signal response. Since characteristics for cleat expansion (and physical damage) produced by mechanical vibration are mainly concentrated on the dynamic aspects of the acoustic wave, these previous methods would be insufficient for the evaluation of current simulation. Therefore, this paper proposed two new parameters, shear wave energy, and variable width, to help further analysis for mechanical vibration. These new parameters are based on wave field information (velocity, stress, and pressure) that measured from simulation grid detectors which located at two main interfaces of cleat model. Figure 6 shows the calculation grids distributed at the main interface of the model.

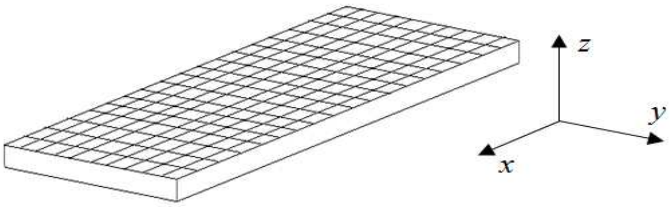

Figure 6. The Sketch of detectors on the model interfaces. Intersection nodes represent the distribution of computational detectors for the value of *SE* and *DW* parameters. The node number at each interface is 151×61(x-y dimension).

3.3.1 Shear wave energy

Polarized waves can be mathematically divided into certain components of compression wave and shear wave. In this research pure compression wave has been used to for incident elastic sub-wave. During the whole simulation area, the shear wave can only be generated in two ways: polarized waves stimulated by an incident wave at interfaces of cleat model, and converted wave that generated by sub-waves' reflection and transmission. Since the converted wave part around the interfaces of that model only exit in a very short time range, the values of shear wave energy (*SE*)

are mainly determined by the polarized wave, which makes it very suitable for evaluation of the magnitude of mechanical vibration. Simultaneously the shear wave component is also very effective to produce physical damage and enhance the CSG desorption amount.

The wave equation (2) that expressed by the theorem of Helmholtz decomposition have the following properties:

$$\nabla \cdot \nabla \times \boldsymbol{\psi} = 0 \, , \nabla \times \nabla \varphi = 0 \, , \tag{13}$$

$$\nabla \times \mathbf{v} = \frac{\partial \mathbf{u}}{\partial t} = \frac{\partial}{\partial t}(\nabla \times \mathbf{u}) = \frac{\partial}{\partial t}(\nabla \times \nabla \times \boldsymbol{\psi}) \, . \tag{14}$$

By using vortex of particle velocity the magnitude of shear wave energy at each detector can be calculated from equation (3) and (4):

$$Es = (\nabla \times \mathbf{v})^2 \, , \quad se = \mu Es^{1/2} \, . \tag{15}$$

For every simulation time step, the total values of shear wave energy at each interface, as equation (16) shows, equal to the parameter *SE*. The value of *SE* is calculated every 0.5μs (every 50 simulation time step) to discuss the changes of wave energy at the interfaces:

$$SE_t = \sum_{j}^{Y} \sum_{i}^{X} se(t, i, j) \, . \tag{16}$$

The *SE* parameter is named shear wave energy in this paper, but it does not represent a kind of real physical energy. This parameter is proposed only to isolate the shear wave component and evaluate the energy changes of the polarized wave at the interface of cleat model. The magnitude of *SE* parameter can accurately indicate the tendency of wave energy changes at the interface, but does not exactly equal to the real wave energy.

3.3.2Variable width of cleats

The permeability of coal samples highly relies on the width of coal cleats because they are the migration pathway for CSG. Based on Darcy's law, the traditional fluid flow in a fracture can be written in equation (17), which indicates that with the constant viscosity μ and pressure gradient flux Q is proportional to the width of fracture b.

$$q = \frac{b^3}{12\mu} \cdot \frac{dp}{dx} \, , \quad Q = lq \quad \text{and} \quad Q = \frac{k_f A}{\mu} \cdot \frac{dp}{dx} \tag{17}$$

Within elastic deformation range, because of various wave dynamic effects at the interfaces of cleat model the constant width b become a function b_c with variables of time and positions that can be written as

$$b' = b + b_c \, , \quad b_c = b_c(x, z, t) \, . \tag{18}$$

So the new fluid formula in a dynamic fracture can be written in equation (19). And

with this equation, the new permeability formula under the wave dynamic can be written in

$$Q^{'} = \frac{1}{L}\int_0^L \int_0^l q \cdot dzdx = \frac{lb^3}{12\mu} \cdot \frac{dp}{dx} + \frac{b^2}{4\mu L}\int_0^L \int_0^l b_c(x,z,t)dzdx, \tag{19}$$

$$Q^{'} = \frac{k_f^{'} A}{\mu} \cdot \frac{dp}{dx}, \quad \overline{k_{fL}^{'}} = k_f + \frac{b^2}{4AL}\int_0^L \int_0^l b_c(x,z)dzdx, \tag{20}$$

$$DW_1 = \int_0^L \int_0^l b_c(x,z)dzdx. \tag{21}$$

By calculating the DW_1 at each time step the variation trends of variable width can be obtained to evaluate the effect of variable width for permeability enhancement. Similarly equation (22) included time domain for the integral of permeability function, which evaluated the overall effect of variable width during a certain simulation time:

$$\overline{k_{fLt}^{'}} = k_f + \frac{b^2}{4AL(T-t)}\int_t^T \int_0^L \int_0^l b_c(x,z,t)dzdxdt, \quad DW_2 = \int_t^T \int_0^L \int_0^l b_c(x,z,t)dzdxdt. \tag{22}$$

In this paper, the time range for DW_2 is the whole simulation range. The Newton-Cotes method is used as numerical integration algorithm.

4. Computational results and discussions

Numerical simulation was carried out with three different models with the following filled media in cleats respectively: water, gas and solid.

4.1 Model one: water-filled cleat

4.1.1 Wave propagation field

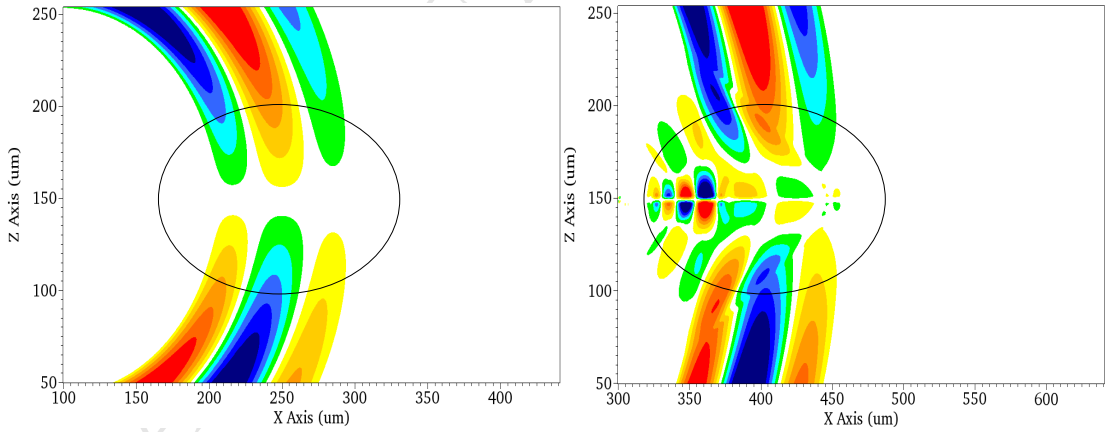

(a) (b)

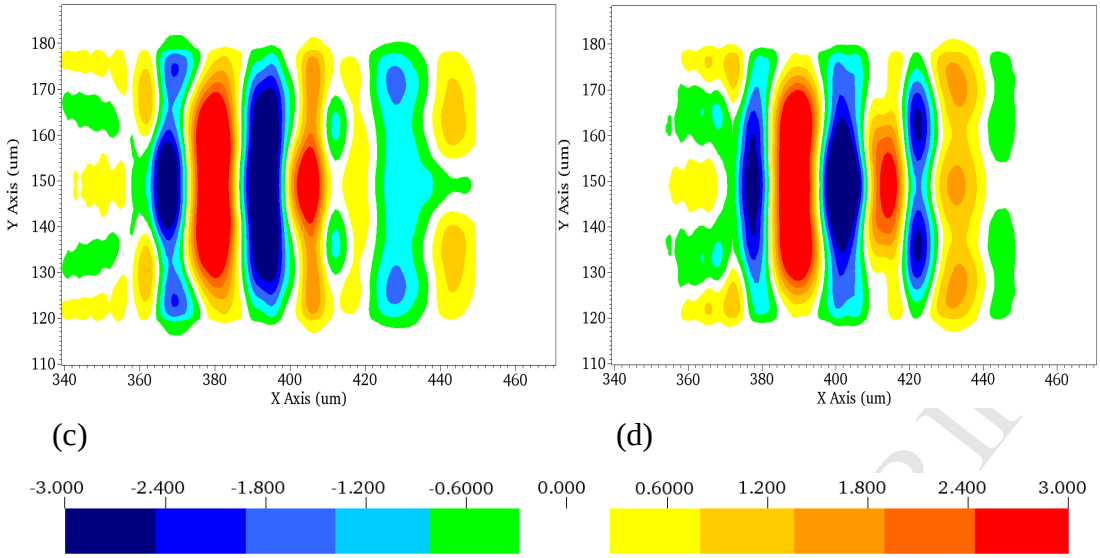

Figure 7. With 0° incident wave angle, V_z component of wave field at different time and dimension (Unit: 1×10^{-2} m/s) (a) $t=9\times10^{-6}$s, (b) $t=2.08\times10^{-5}$s, (c) $t=2.12\times10^{-5}$s, (d) $t=2.13\times10^{-5}$s

With 0° incident wave angle, the propagation of polarized waves at main interfaces of water-filled cleats is a three-dimensional finite low-velocity waveguide. The polarized wave at the fluid-elastic-solid interface can be regarded as Scholte wave, The amplitude or energy concentration reach its maximum at the interface and decreases exponentially away from the interface into both the fluid and the solid medium. Figures 7(a) and (b) show the generation of the polarized wave by using the snapshot of velocity component V_z. As the circle marked in Figure 7(a) indicates the V_z component at the propagation direction parallels to Z axis is the weakest part of incident sub-wave, so it is conspicuous that V_z component in Figure 7(b) becomes much stronger at the fluid-solid interface because of the generation of Polarized waves. Figures 7(a) and 7 (b) also indicate that part of the energy of incident sub-wave has been trapped at the interfaces (energy trapping effect) in the form of the polarized wave, constantly propagating along the interface and partially reflected back at tips of cleat model. Figures 7(c) and (d) exhibits the trapped wave energy at the interface Ⅱ of cleat model in x-y dimension.

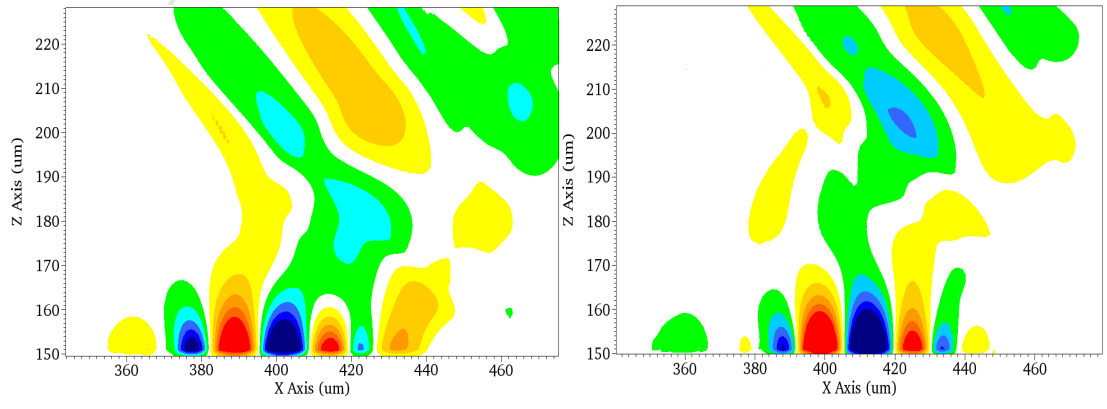

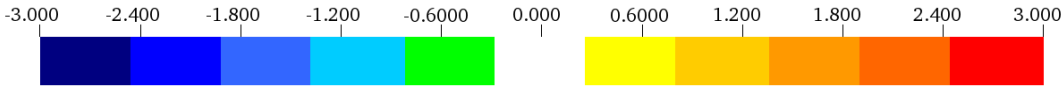

Figure 8.1. Water-filled model with 0° incident wave angle, V_z component represent the energy lost of trapped energy at interfaces of cleat model in 2D (Unit: 1×10^{-2} m/s). (a) t=2.32×10^{-5}s, (b) t=2.45×10^{-5}s

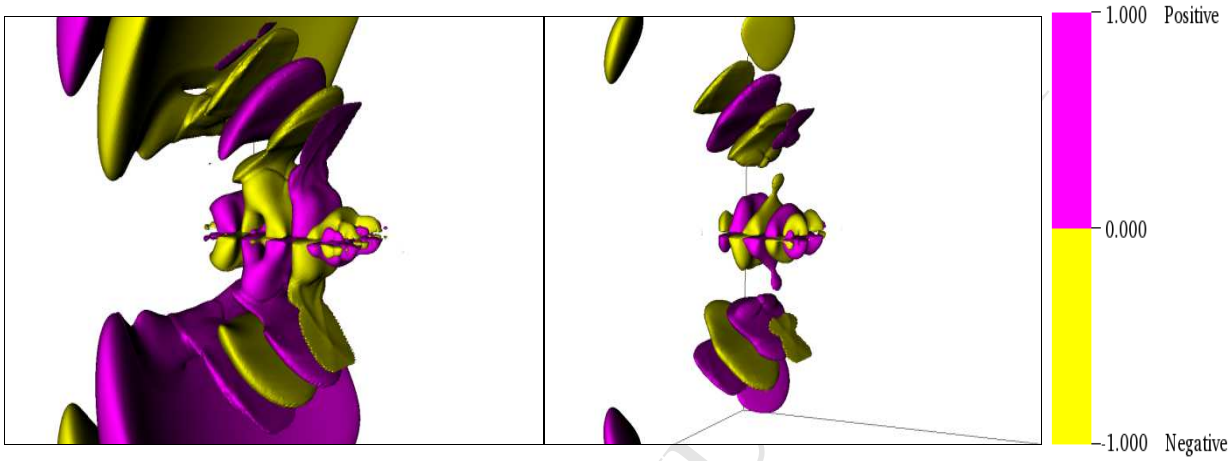

(a) (b)

Figure 8.2. Water-filled model with 0° incident wave angle, V_z component represent the energy lost of trapped energy at interfaces of cleat model in 3D (a) t=2.32×10^{-5}s, (b) t=2.45×10^{-5}s

Figure 8.1 indicates that if considering the whole cleat model as an energy system, energy loss happens at the maximum area of wave constructive interference and cleat model tips in a form of energy groups (Frehner et al., 2010) which are projected to the surrounding medium. Figure 8.2 shows the 3D geometrical shape of these energy groups, which gives clear images of the trapped waves and leaving trend of wave energy at different stages.

4.1.2 *SE* and *DW* measurement

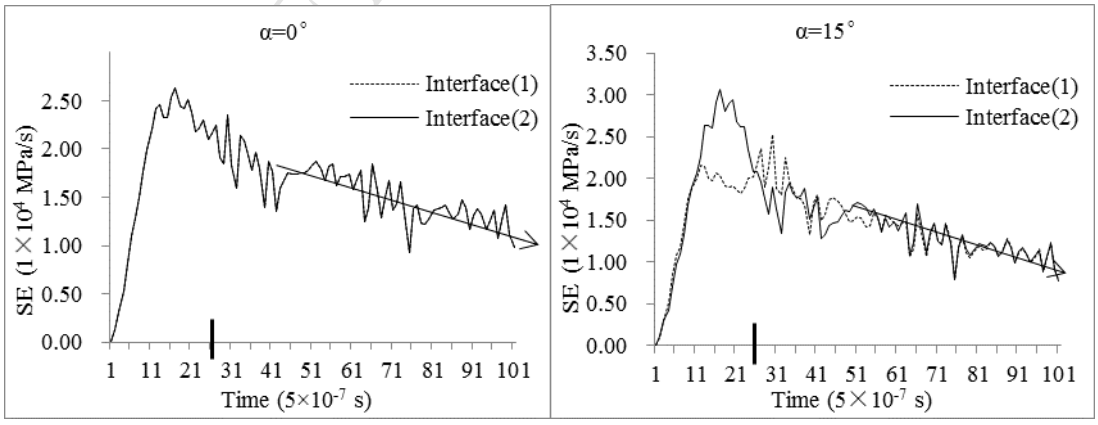

(a) (b)

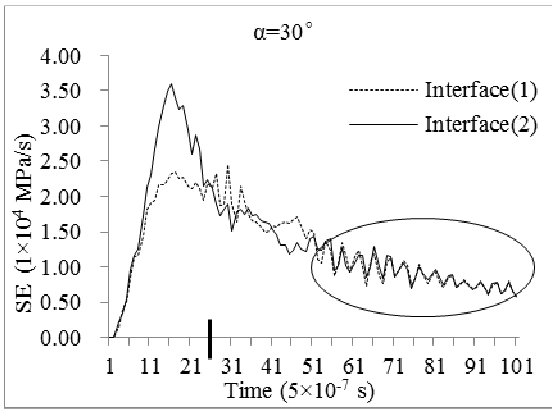

(c)

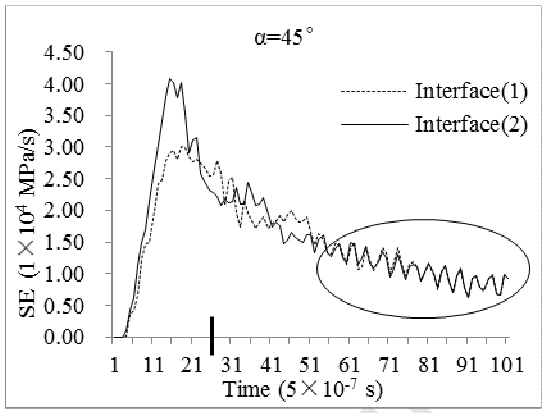

(d)

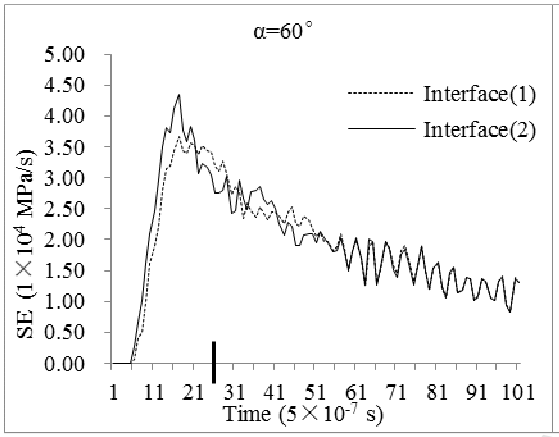

(e)

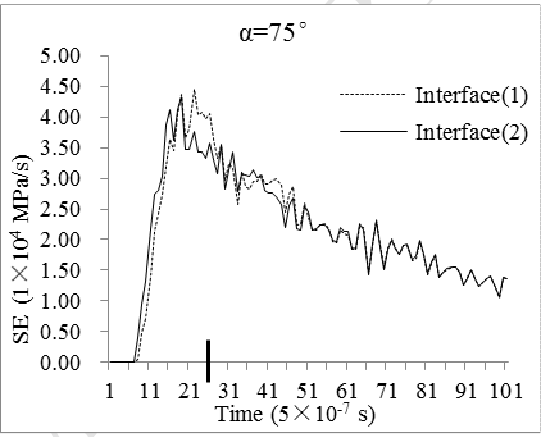

(f)

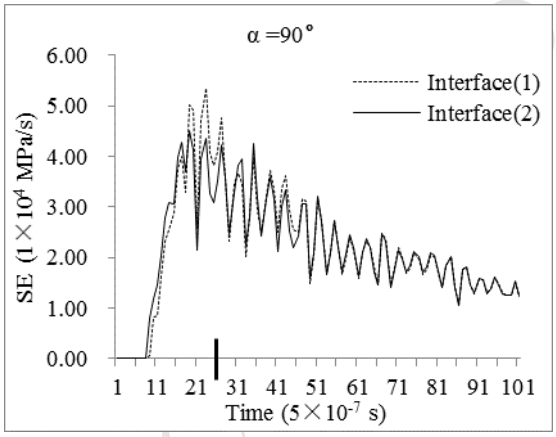

(g)

Figure 9. Water-filled model, the *SE* parameter variation at interface □ and □ with different α values. The thick black short line bars at each horizontal axis represent the start point of leave time.

Figures 9(a) to (g) exhibit the changes of *SE* parameter with time at main interfaces of the cleat model. The bold black marks at each time axis represent the starting time point for incident wave completely left the cleat model, the leave time. Before the mark, with different incident wave angle, the changing pattern of *SE* parameter at the two main faces are quite different; for large angles as in Figures 9(f) or (g), the

patterns are very similar to each other; but for smaller angles Figures 9(a) to (e) the *SE* value in the interface Ⅱ is much high than in the interface Ⅰ at the first, and then the *SE* value at each interface alternatively became the maximum value.

All of the figures in Figure 9 demonstrate the energy trapping effect. After the leave time, the incident sub-wave completely left the model, but the *SE* still maintains at a very high level and gradually loses its energy in a very low rate. Black arrow lines at each Figure 9(a) and (b) indicate that regardless of differences between incident wave angles, all of the energy losing rates are approximately constant value, which is illustrated by straight arrows in Figures 9(a) and (b). The relation between time and energy losing amount can be written in a linear equation:

$$SE = C - K_i t \text{ , } (K_i > 0, t > t_{leave}) \cdot \tag{23}$$

With a serial of sub-waves the energy will constantly accumulate at the cleat model in the form of a polarized wave and when the energy exceed the certain damage threshold the width and distributing area of cleats will be expanded. The energy trapping effect can give a good explanation for the time-accumulative characteristics of desorption amount curve that obtained by Jiang's experiment.

After the leave time, it is noticeable that even various changing patterns of *SE* parameter have been produced by different incident wave angles. The *SE* parameter at each interface gradually becomes equal values. It indicates that the mechanical vibration can equally affect both interface of coal cleats after a short time range (as marked by circles in Figures 9(c) and (d)).

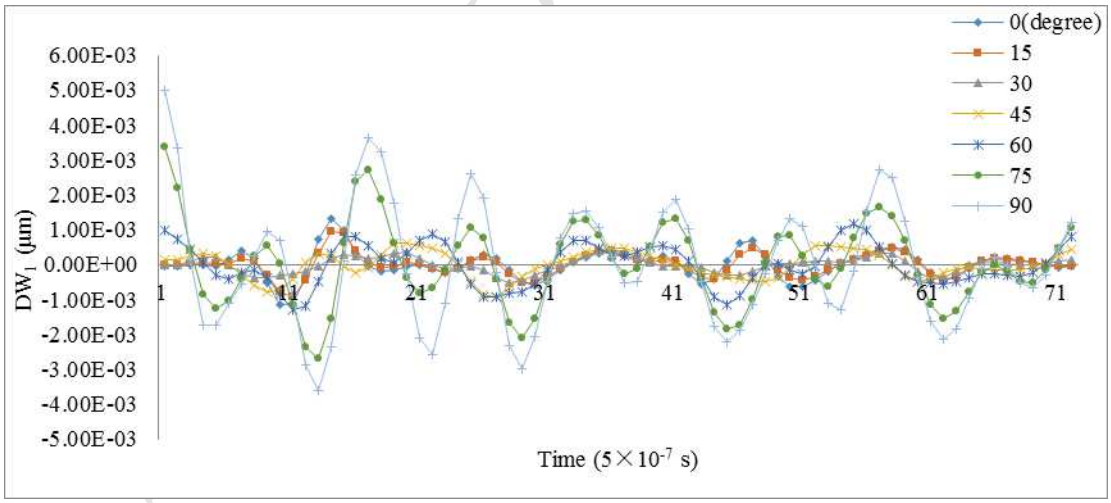

Figure 10. For water-filled model, the DW_1 parameters variation with different α value. The time range is from 2.3×10^{-5}s to 6.0×10^{-5}s.

Figure 10 shows the changes of DW_1 with time under different incident wave angles. Only the part of curves that after the leave time is discussed, to eliminate the impacts of incident sub-wave. As expected the width of cleat model varies with time, which can be divided into two phases: contraction phase and expansion phase. The larger incident wave angle is the more drastic changes for DW_1 values, but the lower

frequency of phases' changes. The variable width is also produced by the polarized wave that trapped at the interface of cleat model, and with the accumulation of wave energy, the value of DW_1 becomes large enough for a strong permeability enhancement.

4.2 Model two: gas-filled cleat

4.2.1 Wave propagation field

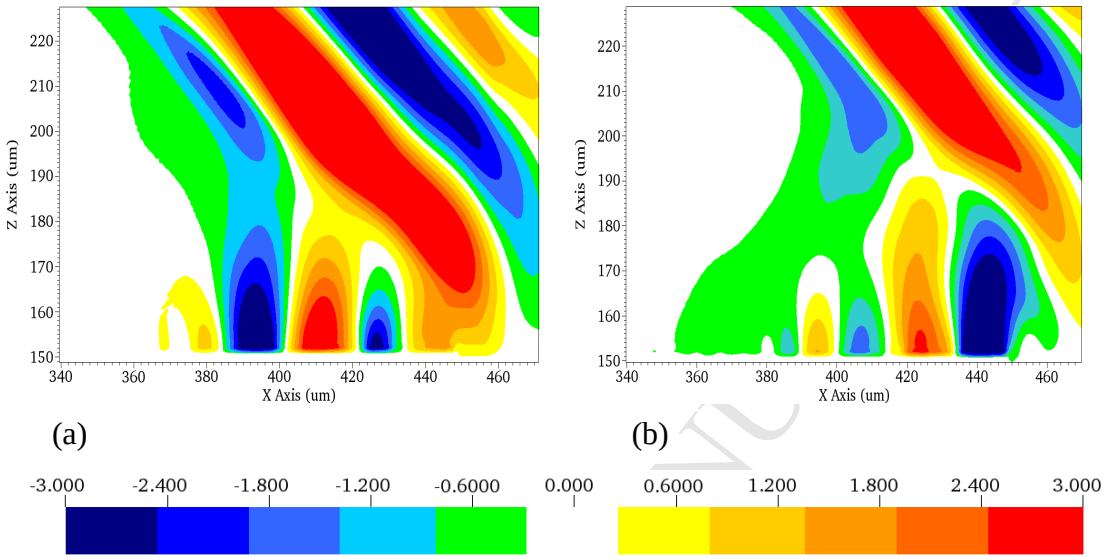

Figure 11.1. Gas-filled model with 0° incident wave angle, V_z component represent the energy loss of trapped energy at interfaces of cleat model in 2D (Unit: 1×10^{-2} m/s). (a) $t=2.32\times10^{-5}$s, (b) $t=2.45\times10^{-5}$s,

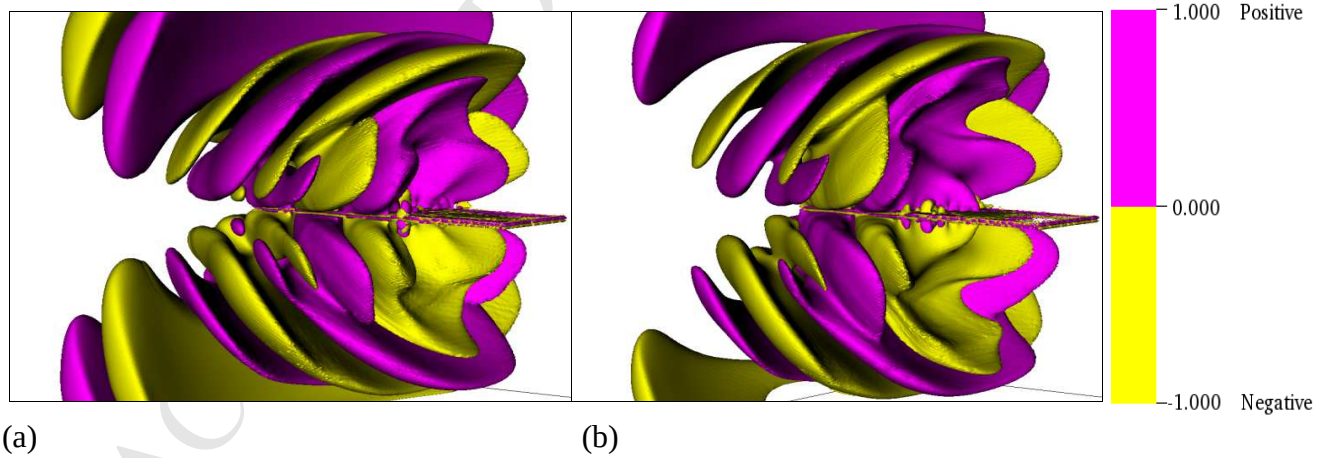

Figure 11.2. Gas-filled model with 0° incident wave angle, V_z component represent the energy loss of trapped energy at interfaces of cleat model in 3D (a) $t=2.32\times10^{-5}$s, (b) $t=2.45\times10^{-5}$s

Figure 11.1 and Figure 11.2 show the modelling results of cleat model filled with gaseous medium. Similarly, the polarized waves are produced at the gas-solid interfaces, which exhibit the energy trapping effect and losing energy by projecting energy groups into the surrounding medium. Figure 11.2(a) and 11.2(b) suggest that unlike water-filled medium the trapped energy for the gas-filled model should have a

high losing rate right before the leave time. Since there is no wave propagation inside the model the energy losing only happens at the maximum area of constructive interference.

4.2.2 *SE* and *DW* measurement

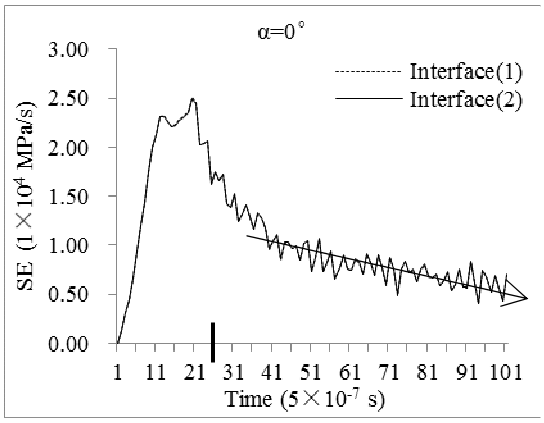

(a)

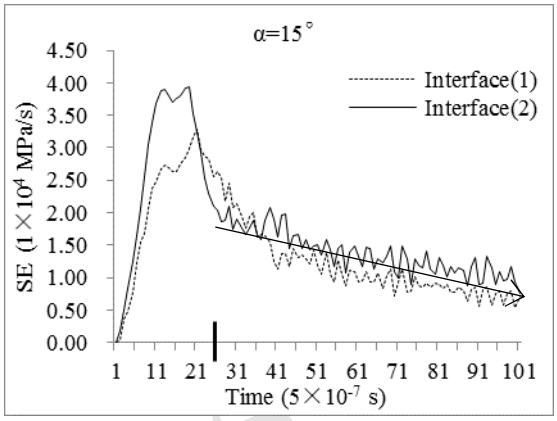

(b)

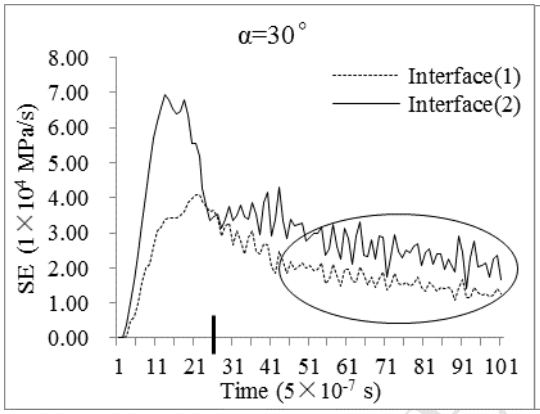

(c)

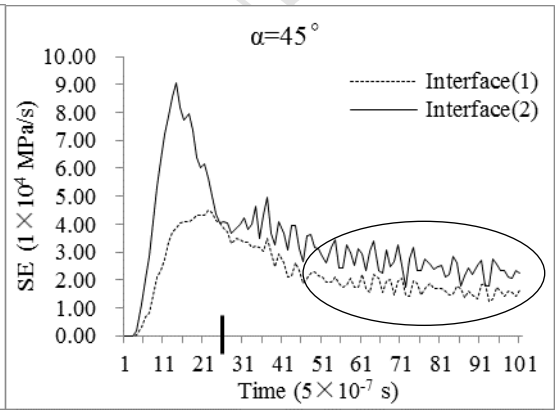

(d)

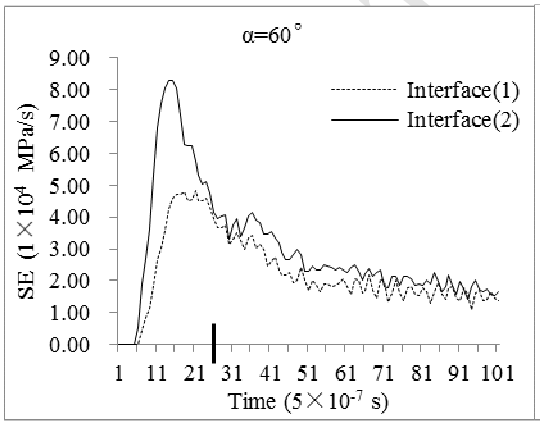

(e)

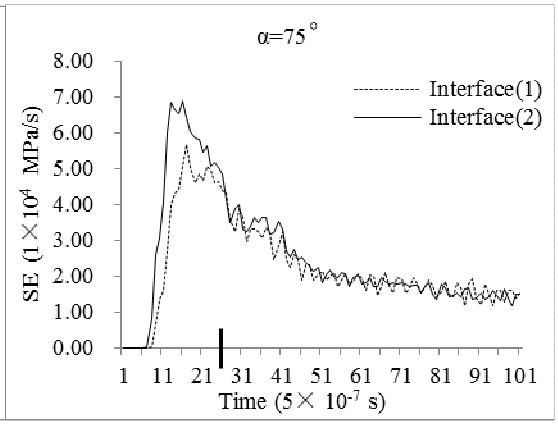

(f)

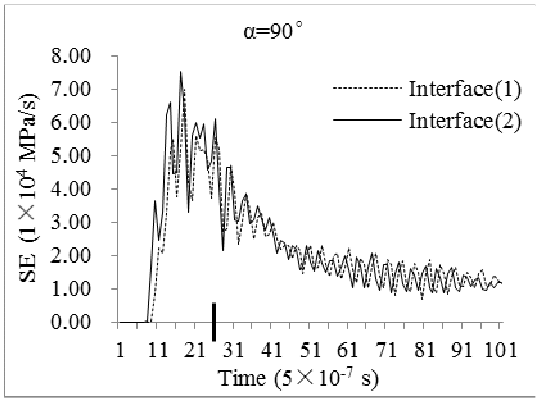

(g)

Figure 12. For gas-filled model, the *SE* parameter variation at interface □ and □ with different α value.

It can be observed from Figures 12(a) to (g) that vibrating pattern also highly affected by incident wave angle, and before the leave time *SE* parameter has the similar characteristics with the water-filled medium. It also demonstrated the phenomenon observed from 3D wave snapshot that there is a period with rapid energy losing rate before the leave time. The rate of energy losing for each interface is approximately the same constant value, but unlike the water-filled medium, smaller incident wave angles make the interface □ maintaining *SE* values that higher than interface □ after the leave time. This phenomenon is marked by circles at Figures 12(c) and (d). These figures indicate that for smaller incident angles, more polarized wave energy will be trapped on the first-arrived interface and keep this advantage all the time. So for a serial incident wave, the physical damage will have a strong preference for the coal cleat interfaces.

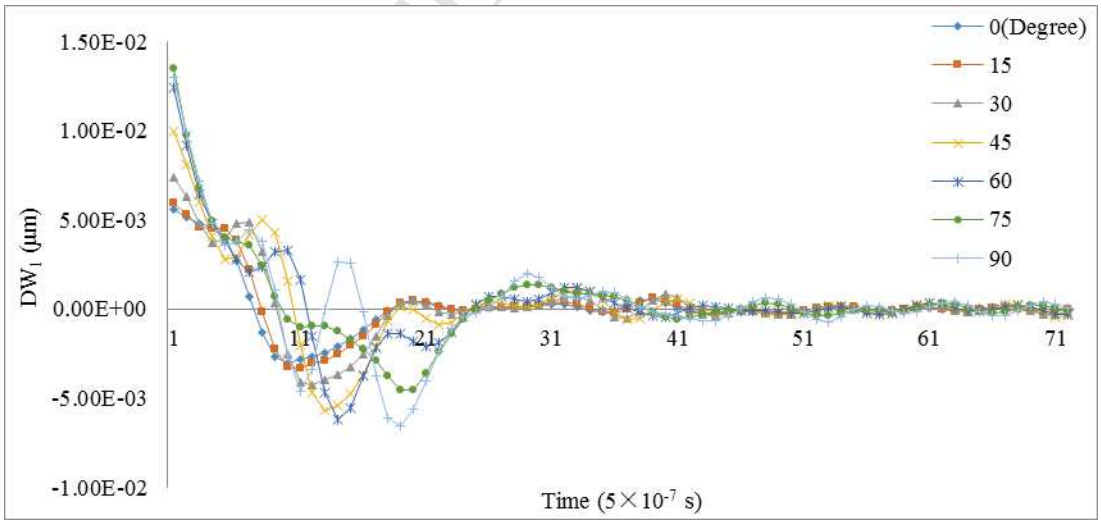

(a)

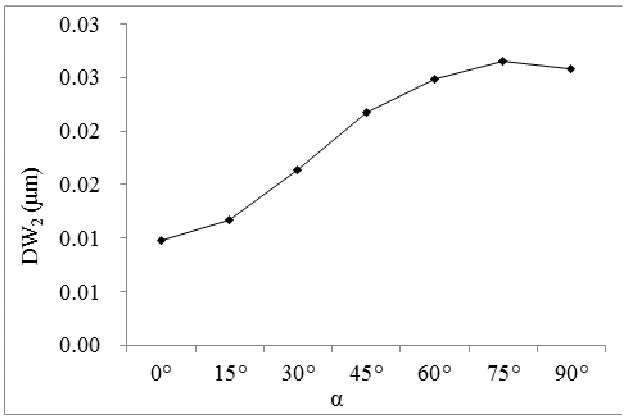

(b)

Figure 13. For gas-filled model, the *DW* parameters variation with different α value. (a) DW_1 parameter, the time range is from 2.3×10^{-5} s to 6.0×10^{-5}s, (b) DW_2 parameter, the time range is the whole simulation time

Figure 13(a) shows the time variation curve of DW_1 parameters for the gaseous model. It indicates that for all the incident wave angles the DW_1 parameters have a dominating maximum value right after the leave time, which is also much high than any DW_1 value for the water-filled model. So it is meaningful to introduce DW_2 parameter to discuss the influence of variable width through the whole simulation time. In Figure 13(b) the DW_2 parameters indicate this expansion trend is increasing with larger α value. Hence, for gas-filled model the width of coal cleats will be highly improved by the stimulation of sub-wave and for larger α value the improvements higher.

4.3 Model three: solid-filled cleat

4.3.1 Wave propagation field

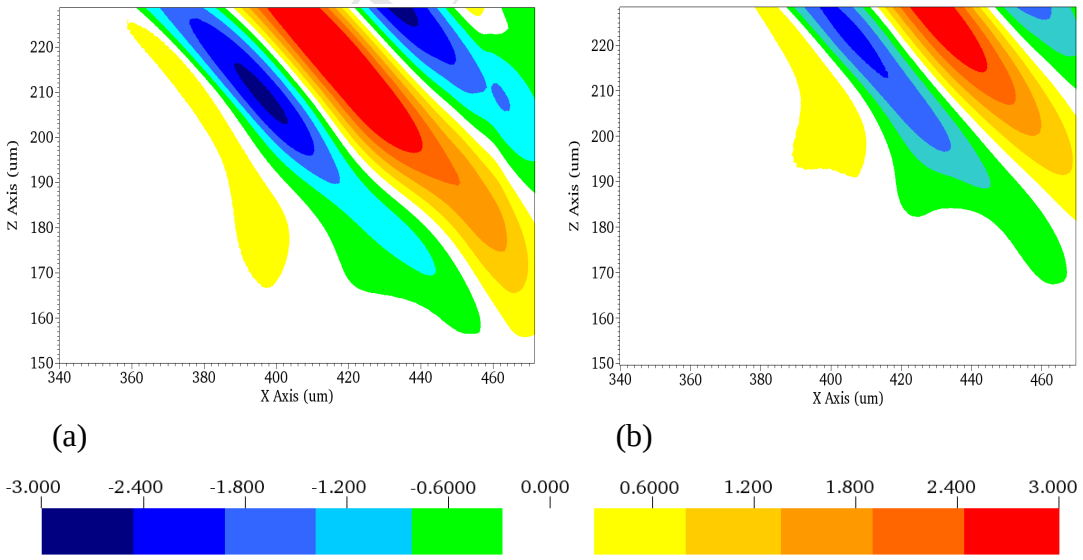

Figure 14.1. Solid-filled model with 0° incident wave angle, V_z component represent the energy lost of trapped energy at interfaces of cleat model in 2D (Unit: 1×10^{-2} m/s). (a) $t=2.32\times10^{-5}$s, (b) $t=2.45\times10^{-5}$s,

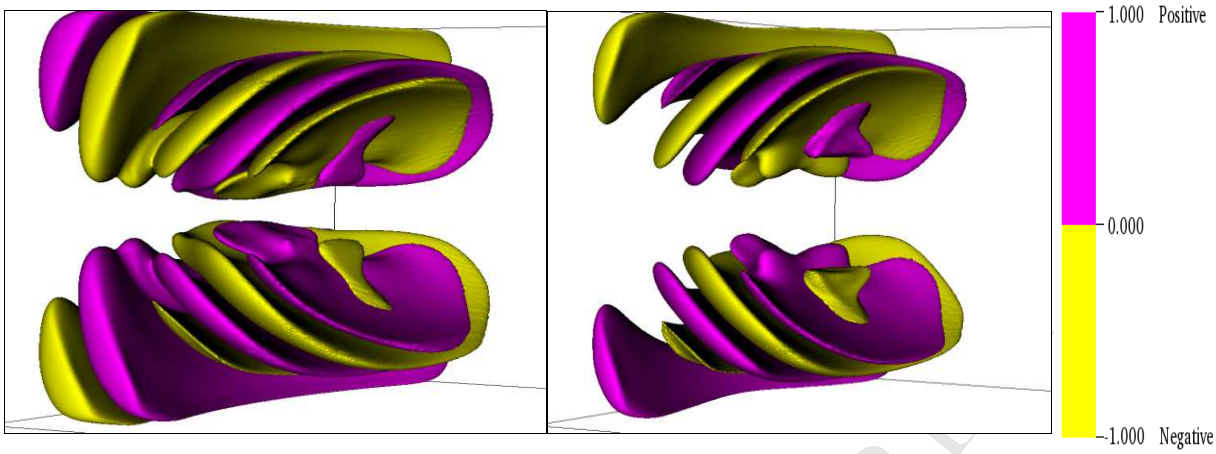

(a) (b)

Figure 14.2. Solid-filled model with 0° incident wave angle, V_z component represent the energy lost of trapped energy at interfaces of cleat model in 3D. (a) t= 2.32×10^{-5}s, (b) t=2.45×10^{-5}s

As a commonly filled medium for coal cleats, calcite has been used as the property of cleat model. Figures 14.1 shows the wave propagation snapshot of solid-filled medium and indicate that there is no obvious energy trapping effect for interface □ and □. This conclusion also can be observed from Figures 14.2 that compare with the water-filled or gas-filled model at the same time step, the wave energy on the interface of the solid-filled model already left the interface.

4.3.2 *SE* parameter measurement

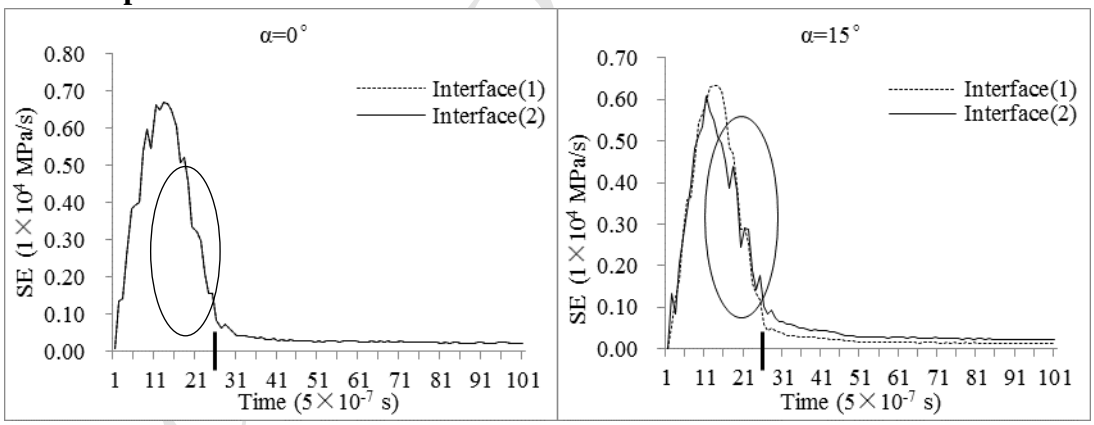

(a) (b)

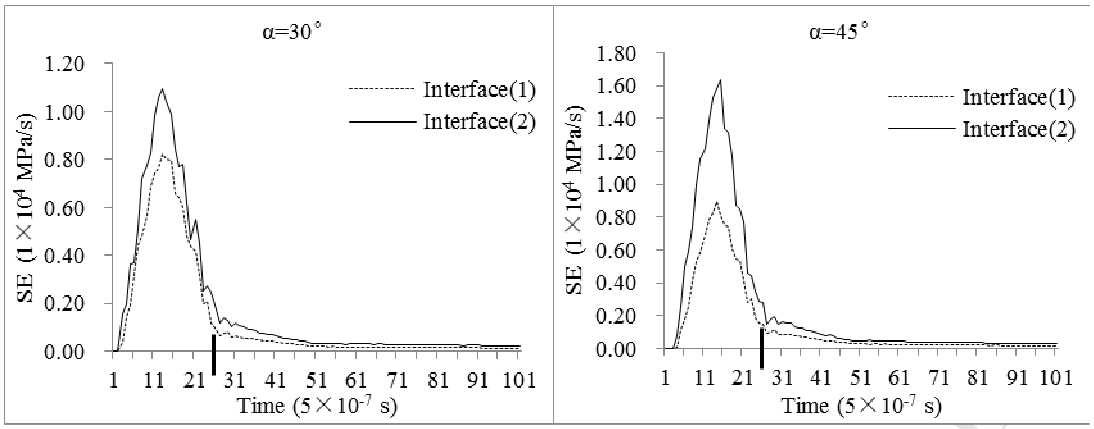

(c)

(d)

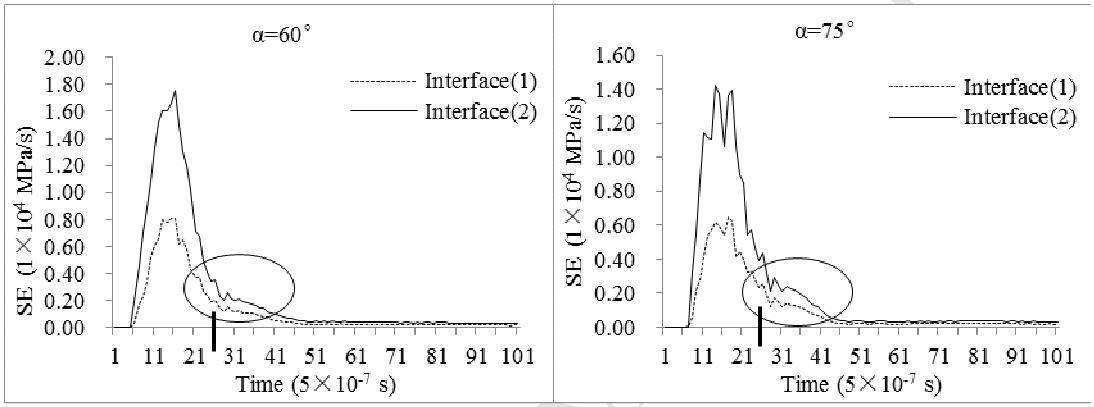

(e) (f)

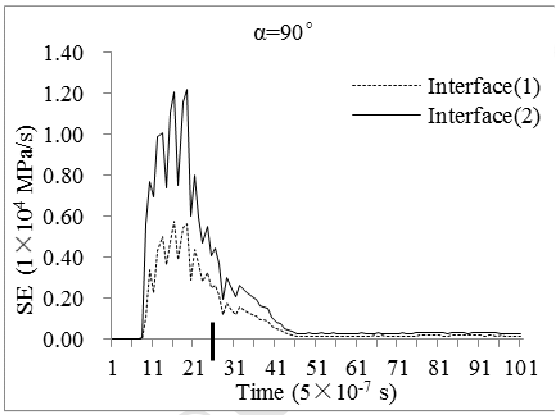

(g)

Figure 15. For solid-filled model, the *SE* parameter variation at interface □ and □ with different α values

Figures 15(a) to (g) for *SE* parameters also suggest that the energy at the main interfaces of model rapidly decaying after the leave time. For large incident angle cases, as the circles in Figures 15(e) and (f), a little amount of energy can be trapped for a very limited time and linearly decay to zero. Hence compare with water-filled and gas-filled models, the energy trapping at the solid model is much smaller for the above cases.

5. Conclusions

Acoustic stimulation is tested in both laboratory and field to enhance the permeability of coal reservoirs, its mechanism is till poorly understood mostly due to the complicities from the heterogeneous fractured coal material itself and its dynamic interaction with incident waves especially along a cleat/fracture inside a coal. As an alternative approach of existing experiment approach, the staggered-grid finite differential method (FDM) is extended and applied to simulate the acoustic stimulation process of coal, and the following conclusions can be drawn:

(1) The dynamic information along the cleat/fracture interfaces and its relationship with the transient permeability are analysed. The shear wave energy (*SE*) and variable width of cleat (*DW*) are successfully introduced and applied to evaluate the acoustic stimulation effects. This forms the theoretical basis for numerical investigation of acoustic stimulation of coal.

(2) Coal cleats and their filled media significantly affects the stimulation results. A coal sample with a cleat/fracture filling with different media of air, water, and weak minerals is successfully simulated and analysed. The simulation results indicate that such mechanical vibration results from the energy trapping ability of coal cleats. This ability is highly affected by the types of filled media (e.g. gas, water, or weak rocks); its existence allows the physical damages to be produced around coal cleats and improve the permeability but highly depends on the cleats and their filled media. For a water or gas-filled cleat, the wave energy is trapped at its interfaces and linearly losing the energy at a very low rate. This effect makes the cleat model trough a long period of mechanical vibration, and can eventually enhance the permeability by producing physical damages at the cleat's neighbouring areas under constant acoustic stimulation. However, for a solid-filled cleat, the trapping effect is much smaller than that with a fluid-filled cleat, so the effectiveness of permeability enhancement is compromised.

(3) The stimulation results also highly depend on the incident waves. The sensitivity analysis of the energy trapping and dynamic variation of fracture width for the cleat/fracture subjected to different incident waves are numerically conducted. Simulation results suggest that the larger incident angles to the cleat orientation are, the larger width of coal cleat, which contributes more to the permeability enhancement of acoustic stimulation.

Overall, the mechanical vibration effects that indirectly observed from the experiments are mainly caused by the energy trapping effect. Such effect is crucial for acoustic stimulation to produce physical damages around coal cleats and enhance the permeability of fractured coal samples, but it is very sensitive to the coal property (i.e. cleats and filled media) and incident wave angles. The numerical simulation could help in obtaining the optimised parameters of stimulation process through the related sensitivity analysis.

References

Achenbach, J.D., 1999. Wave Propagation in Elastic Solid. Netherland. Elsevier

Alhomadhi, E., Amro, M., Almobarky, M., 2014. Experimental application of ultrasound waves to improved oil recovery during waterflooding. Journal of King Saud University–Engineering Sciences. 26: 103-110

Ashour, A.S., 2000. Wave motion in a viscous fluid-filled fracture. International Journal of Engineering Science. 38: 505-515

Azmi, A.S., Yusup, S., Muhamda, S., 2006. The influence of temperature on adsorption capacity of Malaysian coal. Chemical Engineering and Processing: Process Intensification. 45: 392-396

Bakhvalov, N.S., 2001 Courant–Friedrichs–Lewy condition. In Hazewinkel,Michiel, Encyclopedia of Mathematics, Springer

Cenveny, V., Psencik, I., 2006. Energy flux in viscoelastic anisotropic media. International Journal of Geophysics. 166: 1299-1317

Charriére, D., Pokryszka, Z., 2010. Behra P. Effect of pressure and temperature on diffusion of CO2 and CH4 into coal form the Lorraine basin (France). International Journal of Coal Geology. 81: 373-380

Chouet, B., 1986. Dynamics of a Fluid-Driven Crack in Three Dimensions by the Finite Difference Method. Journal of Geophysical Research. 91(B14): 13, 967-13, 992

Frehner, M., Schmalholz, S,M., 2010. Finite-element simulations of Stoneley guided-wave reflection and scattering at the tips of fluid-filled fractures. Geophysics. 75(2):T23-T36

Fuchs, K., Müller, G., 1971. Computation of Synthetic Seismograms with the reflectivity method and Comparison with Observations. International Journal of Geophysics. 23: 417-433

Gandossi, L., 2013. An overview of hydraulic fracturing and other formation stimulation technologies for shale gas production, EUR 26347 Joint Research Centre Scientific and Technical Research series, Publications Office of the European Union, Luxembourg. doi:10. 2790/99937

Hol, S., Peach, C.J., Spiers, C.J., 2011 Applied stress reduces the CO2 sorption capacity of coal. International Journal of Coal Geology. 85: 128-142

Jiang, Y., Song, X., Liu, H., Cui, Y., 2015. Laboratory measurements of methane desorption on coal during acoustic stimulation. International Journal of Rock Mechanics & Mining Sciences. 78: 10-18

Komatitsch, D., Martin, R., 2007. An unsplit convolutional perfectly matched layer improved at grazing incidence for the seismic wave equation. Geophysics. 72(5):SM155-SM167

Korneev, V., 2008. Slow waves in fractures filled with viscous fluid. Geophysics. 73(1):N1-N7.

Levander, A.R., Fourth-order finite-difference P-SV seismograms. Geophysics. 1988; 53(11):1425-1436

Li, Q., Xing, H., 2015. Numerical analysis of the material parameter effects on the initiation of hydraulic fracture in a near wellbore region. Journal of Natural Gas Science and Engineering, 27, 1597-1608

Li, R.C., Kang, J., Qi, Q.X., 2009. The numerical analysis of borehole blasting and application in coal mine roof-weaken. Procedia Earth and Planetary Science. 1: 451-460

Liu, B.X., Xiong, D.G., Xian, X.F., 2006 Adsorption and seepage characteristics of coal to methane under electric field. Journal of Chongqing University. 29: 83-85

Madariaga, R., 1976. Dynamics of an expanding circular fault. Bulleting of the Seismological Society of America. 66(3):639-666

Mohammadian, E., Junin, R., Rahmani, O., Idris, A.K., 2013. Effects of sonication radiation on oil recovery by ultrasonic waves stimulated water-flooding. Ultrasonics. 53: 607-614

Naderi, K., Babadagli, T., 2010 Influence of intensity and frequency of ultrasonic waves on capillary interaction and oil recovery from different rock types. Ultrasonic Sonochemistry. 17: 500-508

Pan, J.N., Hou, Q.L., Ju, Y.W., Bai, H.L., Zhao, Y.Q., 2012. Coalbed methane sorption related to coal deformation structures at different temperatures and pressures. Fuel. 102: 760-765

Robertsson, J.O.A., 1996. Numerical free-surface condition for elastic/viscoelastic finite-difference modeling in the presence of topography. Geophysics. 61(6): 1921-1934

Robertsson, J.O.A., Blanch, O.J., Symes, W.W., 1994. Viscoelastic finite-difference modeling. Geophysics. 59(9):1444-1456

Scholte, J. G., 1947. The range of existence of Rayleigh and Stoneley waves. Geophysical Journal International. 5 (s4): 120-126

Shen, C.M., Lin, B.Q., Zhang, Q.Z., Yang, W., Zhang, L.J., 2012. Induced drill-spray during hydraulic slotting of a coal seam and its influence on gas extraction. International Journal of Mining Science and Technology. 22: 785-791

Shimizu, H., Murata, S., Ishida, T., 2011. The distinct element analysis for hydraulic fracturing in hard rock considering fluid viscosity and particle size distribution. International Journal of Rock Mechanism and Mining Science. 48: 712-727

Virieux, J., 1986. P-SV wave propagation in heterogeneous media: Velocity-stress finite difference method. Geophysics. 51(4): 889-910

Wigginst, R.A., Helmberger, D.V., 1974. Synthetic seismogram computation by expansion in generalized rays. International Journal of Geophysics. 37(1): 73-90

Xiao, X.C., PAN, Y.S., Lu, X.F., 2013. Mechanism of methane permeability enhance through ultrasonic irradiating on low permeable coal seam. Chinese Journal of Geophysics. 56(5): 1726-1733(in Chinese with English abstract)

Ye, G.X., Lu, X.P., Han, P.F., Peng, F., Wang, Y.R., Shen, X., 2008. Application of ultrasound on crude oil pretreatment. Chemical Engineering and Processing: Press Intensification. 47: 2346-2350

Zeng, Y.Q., He, J.Q., Liu, Q.H., 2001. The application of the perfectly matched layer in numerical modeling of wave propagation in poroelastic media. Geophysics. 66(4); 1258–1266

Zhu, J., Popovics, J.S., 2004. Leaky Rayleigh and Scholte waves at the fluid-solid interface subjected to transient point loading. Acoustical Society of America. 116(4), Pt.1:2101-110

Highlights:

- A theoretical explanation for acoustic stimulation induced mechanical vibration effect and coal permeability enhancement.
- Numerical modeling for interface wave field scattering in 3D.
- Mathematical description of wave energy trapping effect at cleat/fracture
- Accurately investigated width change for cleat/fracture under wave field